Van der Waals Interactions in the Hadron Resonance Gas Model

by
Aaron Boggs

A dissertation submitted to the Department of Physics,

College of Natural Sciences and Mathematics

in partial fulfillment of the requirements for the degree of

Bachelor of Science
in Physics

Chair of Committee: Claudia Ratti

Committee Member: Rene Bellwied

Committee Member: Ralph Metcalfe

University of Houston
August 2019

DEDICATION/EPIGRAPH

I dedicate this thesis to TikTok for getting me through my many struggles and hardships while working on this thesis.

ACKNOWLEDGMENTS

Firstly, I would like to thank Dr. Claudia Ratti for supporting me, teaching me and giving me the opportunity to work with her for the past three years. I would also like to thank Paolo Parotto for spending many hours helping me with the work in this thesis and giving me much guidance. They have both taught me so much and I will continue to carry what I have learned from both of them for a long time to come.

Secondly, I would like to thank my family and friends who encouraged me and gave me motivation throughout my time at the University of Houston to continue following my dreams. Without their support, I would not have gotten through the past four years.

ABSTRACT

The Quark-Gluon Plasma (QGP) and its phase transition on the Quantum Chromodynamics (QCD) phase diagram have been at the forefront of high energy physics research for the past few decades. In order to study the QGP and its thermodynamic behavior, many experiments have been undertaken to recreate this state of matter at particle colliders like the Large Hadron Collider (LHC) at CERN and the Relativistic Heavy Ion Collider (RHIC) at the Brookhaven National Laboratory. In addition to experiment, several theoretical models of the QGP have been developed which can then be compared to experimental results. In this thesis, we attempt to successfully implement one of these models, the ideal Hadron Resonance Gas (HRG) model, along with an extension of the model which includes van der Waals type interactions between pairs of baryons and antibaryons, called the Van der Waals Hadron Resonance Gas (VDW-HRG) Model.

In order to determine if our implementations of the two models were successful, we compare our results for several observables at zero chemical potential to the results obtained in [1]. The observables calculated include the system's pressure, energy density, entropy density, the speed of sound, and the specific heat at constant volume. After determining that our implementation of the VDW-HRG model was successful, we then venture out into finite chemical potential and again calculate the system's pressure, energy density, entropy density, number density and the second order fluctuation of baryon number using the VDW-HRG model. Our results at finite chemical potential using the VDW-HRG model qualitatively behave as one would expect them to on the QCD phase diagram, further verifying the success of our implementation.

TABLE OF CONTENTS

LIST OF FIGURES

1 Introduction

1.1 Background

During the first few microseconds after the Big Bang, it is believed that our universe consisted of a quark-gluon plasma (QGP) [6], a high temperature/density phase of strongly interacting matter in which quarks and gluons are liberated from hadrons and are free to move over the entire volume of the system. Through ultra-relativistic heavy ion collisions at various particle accelerator laboratories like the Large Hadron Collider (LHC) at CERN and the Relativistic Heavy Ion Collider (RHIC) at Brookhaven Laboratory, it is possible to recreate this state of matter and study its properties. In order for these accelerators to recreate conditions necessary to form this unique state of matter, very energetic beams of massive ions, such as gold or lead nuclei, are collided head-on at speeds very near the speed of light. The resulting fireball, which can reach a temperature of several trillion degrees kelvin, is the quark-gluon plasma.

From the 1930s through the 1960s, as dozens of new hadrons were being discovered in experiment, it became clear that these "elementary" hadrons must be composed of more fundamental constituents. Several methods were implemented to try to organize and classify all of these new hadrons, the goal being to see if there were more fundamental particles that could explain relationships between similar hadrons. This search led to the proposal of the Eightfold Way by Murray Gell-Mann in 1961 [7] and eventually to the independent proposals of the quark model by both Gell-Mann and George Zweig in 1964 [8, 9]. The Eightfold Way was a method to categorize hadrons based on their spin angular momentum, electric charge and strangeness. In order to better understand why hadrons could be categorized in this way, Gell-Mann and Zweig independently proposed the idea of the quark model. In this model, the fundamental constituents of all hadrons would be smaller particles, called quarks, with fractional electric charge. Gluons would be the force carrying particles for strong interactions, called gauge bosons, who would act as "glue" and hold the quarks together to form hadrons. The quark model also led to the discovery of color charge in strong interactions, where both quarks and gluons have associated color charges. Color charge was

a necessary addition to the theory as there were some hadrons that violated the Pauli exclusion principle, see [10]. The idea of color charge was initially proposed by Oscar Greenberg in 1964 [10] but it wasn't until 1973 when the full formulation of the modern concept of color charge was articulated by Murray Gell-Mann, William Bardeen and Harald Fritzsch.

In normal hadronic matter, the dynamics of quarks and gluons are restricted by what is called color confinement. This mechanism confines the color charged particles, quarks and gluons, within hadrons below a temperature of approximately 2 trillion degrees kelvin, called the Hagedorn temperature. Above this temperature, quarks and gluons undergo another phenomenon called asymptotic freedom. This phenomenon, which was discovered in 1973 by David Gross, Frank Wilczek and David Politzer and who all shared the Nobel Prize in Physics for this breakthrough in 2004 [11, 12], causes strong interactions to become asymptotically weaker as the energy of the interaction gets larger and the interaction distance gets smaller. This discovery was extremely important as prior to its finding, it was believed that quantum field theory interactions suffered from infinitely strong interactions at short distances. These are called Landau poles and make the theories fundamentally inconsistent at small length scales. However, now it is believed that the discovery of asymptotic freedom allows for field theories such as QCD to be completely consistent down to any length scale by eliminating all Landau poles. [1]

The asymptotic freedom phenomenon manifests itself in QCD by allowing for quarks and gluons to break the color confinement rule and become "deconfined" above the Hagedorn temperature mentioned previously. In particle accelerator experiments, this amounts to giving each particle being collided an energy of roughly 175 MeV. Once quarks and gluons have been deconfined and are then liberated from their corresponding hadrons, they form the quark-gluon plasma. The QGP has been shown to behave as an almost perfect fluid with very low viscosity rather than forming a quasi-ideal gas of quarks and gluons [14, 15]. At high densities and low temperatures, the QGP is also believed to behave as a color superconductor [16, 17].

There are two main variables that affect how the QGP behaves: temperature and baryon number

[1] For a brief review of the history and more technical aspects involved with asymptotic freedom, see [13].

density. The standard parameter used to characterize the baryon number density is called the baryon chemical potential (μ_B). The baryon chemical potential is the energy supplied or removed from the system when there is an increase or decrease in the number of baryons and/or antibaryons in the system. One of the current goals of high energy physics is to probe the phase changes of the QGP through variations in both temperature and baryon chemical potential. Variations in other chemical potentials such as electric charge and strangeness can be explored as well but these are not as important to the study of the QCD phase diagram as baryon chemical potential, thus baryon chemical potential is often just referred to as chemical potential.

Gaining a more complete understanding of how the QGP transitions from such high energies to its ordinary hadronic state is essential to learning how our universe evolved in its early stages. Knowledge of this evolution is of great importance to cosmology and also has relevance in the study of Grand Unification Theories (GUTs), which seek to unify the three fundamental forces of nature excluding gravity. Studying the QGP can also teach us much about the physics of regions with high hadronic density such as the cores of neutron stars. There also exists the possibility of exploring technologies using color superconductors in the not too distant future. Much more research still needs to be done on each of these fronts. In the next few sections, various endeavors to further investigate the QGP both theoretically and experimentally will be discussed.

1.2 Lattice QCD

The phase diagram of the QGP has been explored in a few different ways – through experiment, with theoretical models, and through numerical calculations using Lattice Quantum Chromodynamics (Lattice QCD/LQCD). Lattice QCD involves solving the theory of strong interactions, Quantum Chromodynamics (QCD), nonperturbatively on a discrete lattice. The continuum QCD theory can be realized after taking the zero lattice spacing and infinitely large lattice limit. This procedure is extremely computationally intensive and thus requires the use of the largest available supercomputers.

One of the setbacks in studying the QGP phase diagram using numerical methods is that LQCD

is only able to solve the theory of strong interactions at finite temperature and zero baryon chemical potential. Thus, it is only able to investigate the QGP along the y-axis shown in the illustration of the QCD phase diagram in Fig. 1. The reason why Lattice QCD is unable to study the QGP at finite baryon chemical potential is due to the numerical sign problem. This problem refers to the difficulty in solving highly oscillatory integrals in systems with large numbers of fermions, which is the case with the QGP. Now, at zero baryon chemical potential, there is technically a net total of zero fermions as there are equal numbers of baryons and antibaryons in the system, thus LQCD is able to calculate properties of the QGP in this region of the phase diagram.

Despite the numerical sign problem, there are several methods to extend the calculation of observables of the QGP using LQCD to small finite values of baryon chemical potential. One of these methods is to expand thermodynamic quantities into a Taylor series in the baryon chemical potential. The advantage of this method is that one can use calculations of the derivatives of a thermodynamic observable such as pressure at zero chemical potential to obtain the observable's dependence on chemical potential. This allows one to venture out into the T-μ_B plane on the QCD phase diagram without having to suffer from the sign problem. The disadvantage of this technique is that it is not clear a priori how large the values of $\frac{\mu_B}{T}$ in the Taylor expansion can take on for this method to work. In addition, for each thermodynamic observable expanded in this way, the derivatives with respect to the chemical potential must still be calculated, which is most certainly not a trivial task [18]. Another source of uncertainty in this method is that it is unknown how significant the truncation errors are when using just the first few terms in the Taylor series for a specific observable [19].

A second method is to solve the QCD Lagrangian using imaginary values of chemical potential rather than using real values. This approach allows for Monte Carlo techniques to be used in simulations of Lattice QCD. After this is done, one can analytically continue these results to real values of μ_B. However, there are difficulties and unsolved problems with this method. A more in depth discussion of these issues as well as an explanation of several other methods used to calculate observables with LQCD can be found in [20].

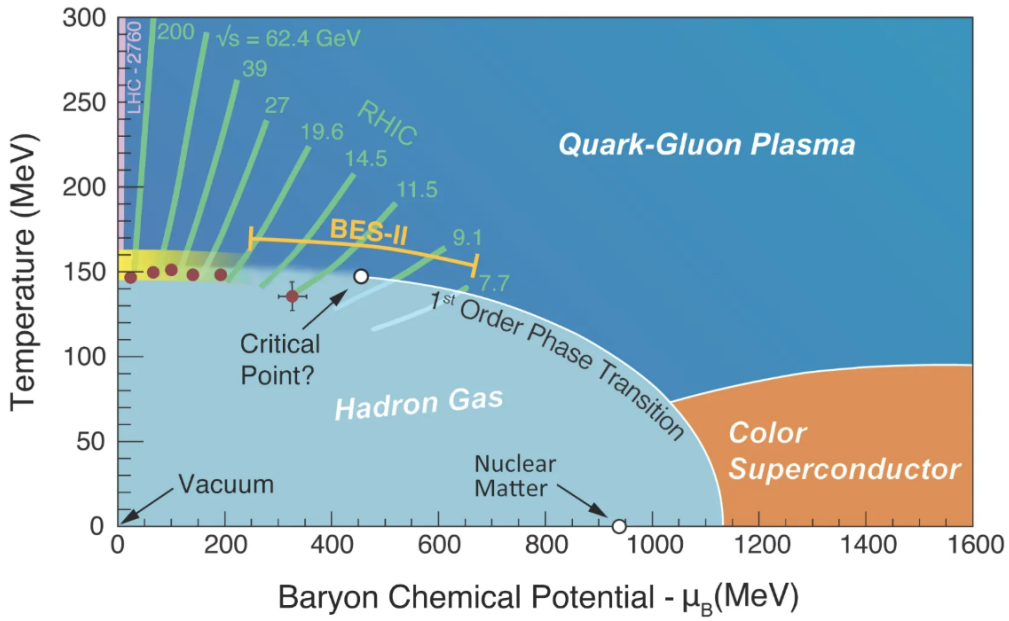

Figure 1: Illustration of the QCD phase diagram.

1.3 Experiment

The existence of the QGP was first proposed in the mid-1970s by two independent research groups [21, 22]. These proposals were made just ten years after the conception of the Quark Model [8, 9] and just two years after the prediction of the existence of asymptotic freedom in QCD [11, 12]. Shortly after the idea of the QGP was proposed, the particle physics community began adapting existing high energy proton accelerators into incorporating heavy ion nuclear beams. Heavy ions were needed as in order to study the thermodynamic behavior of the QGP, the system must behave like 'matter', as opposed to individual elementary particles, and also be in equilibrium so that thermodynamic quantities such as pressure and energy density can be defined along with an equation of state that relates these quantities. Collisions of protons produced too few resultant particles to meet these requirements whereas collisions between heavy nuclei allow for enough particles to be created for a long enough lifetime so that the system can reach equilibrium and thus allow for its thermodynamics to be studied.

By the 1980s, these ultra-relativistic heavy ion nuclear beams were ready to begin investigations

into the proposed QGP phase of matter in the laboratory. The first active experiments searching for the QGP began running simultaneously in 1986 at the Super Proton Synchrotron (SPS) at CERN and at the Alternating Gradient Synchrotron (AGS) at Brookhaven National Laboratory. At AGS, silicon and gold nuclei were collided at energies of 10 GeV/nucleon [23]. The first nuclear collisions at CERN actually started in the early 1980s when helium nuclei, called alpha particles, were accelerated to center-of-mass energy per nucleon-nucleon pair $\sqrt{s_{NN}} = 64$ GeV at the Intersecting Storage Rings (ISR) accelerator. In 1986, CERN began injecting oxygen nuclei into the SPS at an energy of 200 GeV/nucleon ($\sqrt{s_{NN}} = 19.6$ GeV) [23, 24, 25]. Experiments at CERN began ramping up in the '90s as upgrades were made at several of CERN's accelerators to accomodate a new lead ion source. All of this work culminated in 2000 when CERN announced that circumstantial evidence had been found for the creation of a new state of matter in their Pb+Pb collisions at the SPS accelerator [26].

Meanwhile at Brookhaven, proposals for a new heavy ion collider that would accelerate gold nuclei up to $\sqrt{s_{NN}} = 200$ GeV was submitted in 1984 and eventually led to the construction of the Relativistic Heavy Ion Collider (RHIC) which would begin running experiments in 2000. Although evidence had been found for the QGP at CERN in 2000, it was not until 2005 when the real discovery of the QGP took place as four international collaborations who had been studying the gold nuclei collisions at RHIC announced their results from the first five years of measurements [27, 28, 29, 30]. Moreover, the results showed a number of unexpected properties of the QGP such as jet quenching, heavy-quark suppression and an indication that the QGP behaves as a nearly perfect fluid with very small shear viscosity [31].

One of the most active fields of research is exploring the phase diagram of the QGP, as mentioned previously in Section 1.1. The investigation of the phase boundary of the QGP along with the search for the critical point on the phase diagram began in 2010 with the Beam Energy Scan (BES) program at RHIC. As its name suggests, the BES program was created to scan different beam energies which in turn allows for the investigation of various parts of the phase diagram. In order to scan regions of the diagrams with large chemical potential, a smaller collision energy must be

used than the collision energies needed to probe smaller chemical potentials. This is because at lower collision energies, the baryons in the beam spend a longer time in the "interaction zone" and thus leave an excess of baryons in the ensuing fireball which results in a larger net baryon density and chemical potential. Conversely, at higher collision energies, the baryons spend less time interacting and thus the fireball has a lower baryon content resulting in a lower chemical potential.

The BES program was split into two different phases, BES-I and BES-II. The BES-I program ran from 2010 to 2014 and had three main goals: to investigate the turn-off signatures of the QGP, to search for a possible first order phase transition between hadronic matter and the QGP, and to search for a potential critical point. The final results for BES-I can be found in Refs. 21-25 of [32]. Several promising results were reported, however statistical uncertainties, especially at low energies, limit the ability for any conclusive results to be ascertained. The goal of the BES-II program, which is to run from 2019 to 2020, is to decrease these uncertainties by increasing detector performance and extend the scanning to lower beam energies and thus higher chemical potentials. Brief reviews of the entire BES program can be found in [32, 33].

1.4 Theoretical Models

The third and final method used to understand the QGP, which is also the most relevant to the work being presented in this thesis, is through investigating theoretical models. Even before the idea of the existence of quarks and gluons had been put forward in the mid-60s by Gell-Mann and Zweig, particle physicists had already begun creating models to better understand what happens when hadrons are subjected to extreme temperatures and densities such as those found in the QGP. One of the first models was published in 1961 by future Nobel Prize winner, Dr. Yoichiro Nambu, and Dr. Giovanni Jona-Lasinio, thus the model is called the Nambu Jona-Lasinio Model (NJL) [34]. This model was important as it was able to successfully account for chiral symmetry breaking [35], however, it is not able to model color confinement and is not renormalizable in four spacetime dimensions. Thus, the NJL model is limited to being an effective field theory substitute for low

energy QCD.

Another important theoretical model that became popular in the 70s and 80s was the MIT Bag model. In 1974, a group of physicists working at Massachusetts Institute of Technology proposed the idea for the Bag model, now known as the MIT Bag model [36]. This model was important as it modelled color confinement by suggesting that, when quarks and gluons are placed in the QCD vacuum, the vacuum will expel the color fields of the quarks and gluons and confine them to a small finite region of space, called a "bag". In this region of space, there would exist a constant, positive potential energy that allows the quarks and gluons to move freely without being in a color singlet state. Most of the research on the MIT Bag model ceased after the 1980s as more successful approaches to studying hadrons through theoretical models were developed.

The most important model currently and the one most relevant to the work done in this thesis is called the Hadron Resonance Gas (HRG) model. The idea behind the model was initially conceived by Dr. Rolf Hagedorn in 1965 and it was in this paper that he proposed two fundamental ideas: that hadrons had an exponentially increasing mass spectrum, and that modelling the hadrons and their resonances as a non-interacting gas would be equivalent to modelling an interacting gas of only ground-state hadrons. The first idea led Hagedorn to realize there could be a limiting temperature for nuclear matter, which later came to be called the Hagedorn temperature. The second idea led to the formulation of the Hadron Resonance Gas model: a thermal system of ideal, non-interacting particles that includes all experimentally known hadrons and their resonances.

Over the past few decades, the ideal HRG model has shown remarkable agreement with both Lattice QCD and experimental results, up until the transition temperature. At this point, deviations in many thermodynamic quantities start to appear. This has led to the development of many variations of the ideal HRG model which attempt to take into account various phenomena, not covered in the ideal case, in an attempt to reduce the deviations from lattice and experimental data.

One of the first and most important modifications to the ideal HRG model was the inclusion of repulsive forces between hadrons due to their finite size. This take on the ideal model is called

the Excluded Volume HRG (EVHRG) model and has been explored extensively. Recently in 2017, an extension of the EVHRG that includes an additional van der Waals type attractive interaction between hadrons began to be explored more extensively. This model, which combines both finite hadron volumes as a repulsive force in addition to an attractive force, is called the Van der Waals HRG (VDW-HRG) model. In this thesis, the VDW-HRG model will be explored and compared to the ideal HRG model and to Lattice QCD results.

1.5 Outline

The main goal of this thesis was to successfully incorporate van der Waals interactions into the ideal Hadron Resonance Gas model and then compare the results for several thermodynamic observables to Lattice QCD and ideal HRG model data. In Chapter 2, the methodology of implementating both the ideal HRG model and the VDW-HRG model will be presented. In Sec. 2.1, the ideal HRG model will be described and in Sec. 2.2, the process on how to include van der Waals interactions between pairs of baryons and antibaryons will be described. Section 2.3 will describe specifically how the models were implemented and how the results were calculated and found.

In Chapter 3, results will be presented for several thermodynamic observables using both the ideal HRG and VDW-HRG models. In Sec 3.1, results at zero chemical potential for select observables calculated using the ideal and VDW-HRG models will be shown and compared with results for the same observables from [1]. This comparison will allow us to determine if our implementations of the models were successful. In Sec. 3.2, results for some of the observables presented in Sec. 3.1 will be given except this time, the results will only be from the VDW-HRG model and will use finite chemical potential. Finally, in Chapter 4, conclusions on the results and analysis of the work presented in this thesis will be given.

2 Methodology

2.1 Hadron Resonance Gas Model

In the ideal Hadron Resonance Gas (HRG) model, the system consists of non-interacting, point-like hadrons and their resonances. The logarithm of the partition function of a hadron resonance gas in the grand canonical ensemble can be written as

$$lnZ^{id} = \sum_i lnZ_i^{id} \tag{1}$$

where the sum is over each hadronic state and the id refers to the non-interacting, ideal HRG model. For each hadron and its associated resonances, the individual particle partition function is given by

$$lnZ_i^{id} = \pm\frac{Vg_i}{2\pi^2}\int_0^\infty p^2dp\, ln[1 \pm \exp(-(E_i - \mu_i))/T)] \tag{2}$$

where V is the total volume of the system, g_i are the individual degeneracies of each particle, p is momentum, $E_i = \sqrt{p^2 + m^2}$ is the energy of each particle where m is the particle's mass, and finally $\mu_i = B_i\mu_B + S_i\mu_S + Q_i\mu_Q$ is the total chemical potential where B_i, S_i, and Q_i are the baryon number, strangeness, and charge associated with each particle and the μ_B, μ_S, and μ_Q are the associated chemical potentials. The pressure p^{id}, energy density ε^{id}, and the number density n^{id} of the system in the ideal HRG model are given by the following equations,

$$p^{id} = \sum_i(\pm)\frac{g_iT}{2\pi^2}\int_0^\infty p^2dp\, ln[1 \pm \exp(-(E_i - \mu_i))/T)], \tag{3}$$

$$\varepsilon^{id} = \sum_i \frac{g_i}{2\pi^2}\int_0^\infty \frac{p^2dp}{\exp[(E_i - \mu_i)/T] \pm 1}E_i, \tag{4}$$

$$n^{id} = \sum_i \frac{g_i}{2\pi^2}\int_0^\infty \frac{p^2dp}{\exp[(E_i - \mu_i)/T] \pm 1}. \tag{5}$$

The upper and lower signs in Eqs. (2)-(5) correspond to fermions and bosons, respectively. After we find either the partition function or the pressure of the system, other thermodynamic quantities can be calculated.

2.2 Including van der Waals interactions

The van der Waals (VDW) equation of state is a thermodynamic model that allows one to calculate the pressure for systems of particles in equilibrium that have both attractive and repulsive interactions. The VDW model is applicable to the QGP as it is able to describe a first order liquid-gas phase transition that ends at a second order phase transition point, called the critical point. This behavior is exactly what is expected to occur in the QCD phase diagram.

In the canonical ensemble, where the independent variables of the system are the temperature T, volume V and the number of particles N, the VDW equation of state takes the form,

$$p(T,n) = \frac{NT}{V-bN} - a\frac{N^2}{V^2} \equiv \frac{nT}{1-bn} - an^2 \tag{6}$$

where $p(T,n)$ is the pressure of the system, $n \equiv N/V$ is the number density of the particles within the system, and a and b are the VDW parameters that describe the attractive and repulsive interactions respectively. The first term on the right hand side of Eq. (6) corresponds to the excluded volume (EV) correction which replaces the total volume of the system with the available volume, i.e. it subtracts out the volume being taken up by the particles. The available volume of the system is then given by $V_{av} = V_{tot} - bN$ where $b = \frac{16}{3}\pi r^3$ and r is the radius of each particle. The second term on the right hand side describes the attractive interaction between particles and comes from the mean field of the system.

The main issue with formulating the VDW model using the canonical ensemble is that in the canonical ensemble, the number of particles, N, is fixed. If we want to investigate the thermodynamics of a system where the number of particles fluctuates, like the QGP, we need to formulate the VDW model in terms of the grand canonical ensemble. In the grand canonical ensemble, the

pressure is defined in terms of the temperature and chemical potential and thus can account for particle fluctuations. The van der Waals equation of state in the grand canonical ensemble can be written as [37, 5],

$$p(T,\mu) = p^{id}(T,\mu^*) - an^2 \tag{7}$$

$$\mu^* = \mu - bp(T,\mu) - abn^2 + 2an \tag{8}$$

where n is the particle number density and can be defined in the grand canonical ensemble as

$$n(T,\mu) \equiv \left(\frac{\partial p}{\partial \mu}\right)_T = \frac{n^{id}(T,\mu^*)}{1 + bn^{id}(T,\mu^*)}. \tag{9}$$

The terms $p^{id}(T,\mu^*)$ and $n^{id}(T,\mu^*)$ in Eq. (7) and (9) are the pressure and number density calculated using Eqs. (3) and (5) with the ideal HRG model but now using the modified chemical potential, μ^*, defined in Eq. (8). In order to solve for the pressure and number density in the HRG model that now includes van der Waals interaction, which from now on will be called the VDW-HRG model for short, Eqs. (7)-(9) must be solved numerically as they are each transcendental equations.

After the pressure and number density in Eqs. (7) and (9) are solved for numerically as functions of the temperature T and chemical potential μ, other important thermodynamic quantities can be calculated. One of these quantities, the entropy density, can be found for a van der Waals gas and can be calculated using,

$$s(T,\mu) \equiv \left(\frac{\partial p}{\partial T}\right)_\mu = \frac{s^{id}(T,\mu^*)}{1 + bn^{id}(T,\mu^*)}, \tag{10}$$

where $s^{id}(T,\mu^*)$ is calculated by taking the partial derivative of $p^{id}(T,\mu^*)$ with respect to the temperature at constant chemical potential. Thus, the expression for $s^{id}(T,\mu^*)$ is

$$\begin{aligned} s^{id}(T,\mu^*) \equiv \left(\frac{\partial p^{id}}{\partial T}\right)_\mu = \sum_i \Bigg[(\pm)\frac{g_i}{2\pi^2}\int_0^\infty p^2 dp\, ln[1 \pm \exp(-(E_i-\mu_i))/T)] + \\ \frac{g_i}{2\pi^2 T}\int_0^\infty p^2 dp \frac{(E_i-\mu_i)\exp(-(E_i-\mu_i))/T)}{1 \pm \exp(-(E_i-\mu_i))/T)}\, ln[1 \pm \exp(-(E_i-\mu_i))/T)] \Bigg]. \end{aligned} \tag{11}$$

The energy density for a van der Waals gas is given by

$$\varepsilon(T,\mu) = \frac{\varepsilon^{id}(T,\mu^*)}{1+bn^{id}(T,\mu^*)} - an^2 \tag{12}$$

where $\varepsilon^{id}(T,\mu^*)$ is found using Eq. (4) with the modified chemical potential from Eq. (8). An alternate way to find the energy density in the VDW-HRG model using the grand canonical ensemble is given by

$$\varepsilon(T,\mu) = Ts + \mu n - p \tag{13}$$

where s, n and p are the observables from the VDW-HRG model defined in Eqs. (7), (9) and (10). Other important quantities include the specific heat at constant volume which is defined as

$$C_V = \left(\frac{\partial \varepsilon}{\partial T}\right)_V \tag{14}$$

and the susceptibilities of conserved charges which are defined as

$$\chi^{xyz}_{BSQ} = \frac{\partial^{x+y+z}(p/T^4)}{\partial(\mu_B/T)^x \partial(\mu_S/T)^y \partial(\mu_Q/T)^z}. \tag{15}$$

2.3 Implementation

As mentioned in Sec. 1.5, the goal of this thesis was to successfully implement the VDW-HRG model, which consists of incorporating van der Waals interactions into the ideal HRG model. This idea has been proposed and implemented before in several works [1, 38, 39, 40, 41]. In this thesis, the success or failure of our implementation will be determined by comparing this work to the work that was done using the VDW-HRG model in [1].

In order to make a valid comparison, we must follow the same procedure adhered to by [1]. Firstly, the same van der Waals parameters, a and b must be used in each case. In [1], the van der Waals parameters used were found by using LQCD data [42, 43] for the pressure, energy density, entropy density, specific heat at constant volume, and the second order baryon number

susceptibility, and fitting this data at $\mu_B = 0$ within the temperature range 130-180 MeV with the VDW-HRG model. To extract the values of a and b, a χ^2 minimization technique was used. With this procedure, the best fit values for the two van der Waals parameters were found to be a=1250 $\pm$ 150 MeV fm^3 and r=0.7 $\pm$ 0.05 fm where the van der Waals parameter b=$\frac{16}{3}\pi r^3$. These values are significantly higher than those found in [5] where the values for a and r were estimated to be 329 MeV fm^3 and 0.59 fm respectively. This discrepancy can be attributed to the fact that in [5], the VDW parameters were extrapolated by reproducing the properties of nuclear matter in its ground state, (see Ref [44]), as opposed to fitting the VDW-HRG model with LQCD data. In Sec. 3.1, results for different observables will be shown using both the VDW parameters found by [1] and those found by [5].

It is important to note that it was assumed in both [5] and [1] that the van der Waals parameters are not dependent on temperature and chemical potential. It is also implied that hadron masses are independent of temperature and that the magnitude of the attractive and repulsive interactions are the same for all pairs of baryons and antibaryons which would not be the case in reality. These may very well be significant assumptions that must be relaxed in order to compensate for deviations that still exist between VDW-HRG and LQCD/experimental results. [2,3]

The first step taken in implementing the VDW-HRG was importing data for all known hadrons and their resonances into Mathematica. Following in the footsteps of Samanta and Mohanty [1], the 2016 Particle Data Group listing of all known hadrons and their resonances up to a mass of 3 GeV is used in this analysis [46]. The data was imported and separated according to baryon number, thus giving separate data matrices for baryons, antibaryons, and mesons. Next, the formulas for pressure, number density, energy density and entropy density were written out using Eqs. (3)-(5) and (7)-(12). For each of these observables, we need to extract the mass, degeneracy, and baryon number for each particle from the data matrices for baryons, antibaryons and mesons as these three

[2]Recently, work has been done on relaxing some of these assumptions such as making a, the attractive VDW parameter, temperature dependent[39], incorporating temperature dependent hadron masses [45], and having unique VDW parameters specified for each pair of particle species [41].

[3]It has also recently been shown that both VDW parameters, a and b, are in fact dependent on the beam energy and hence are dependent on temperature [38].

properties are needed in the formulas for each observable. In addition, we need to sum over all hadrons used. To do this, a module inside of Mathematica was made for each observable such that these conditions were met.

The next difficult part was figuring out how to numerically find the non-ideal, VDW pressure and number density using the modified chemical potential. Essentially, the issue is that the modified chemical potential, see Eq. (8), is a function of the non-ideal VDW pressure and number density, Eqs. (7) and (9), respectively and both the VDW pressure and the number density are also functions of the modified chemical potential. Thus, numerical root finding has to be used in order to solve for solutions of these three equations simultaneously. For each observable, this root finding needed to be done separately for baryons and antibaryons as the modified chemical potential is dependent on the baryon number. However, because we assume mesons are non-interacting in this analysis, the mesons are only treated using the ideal Hadron Resonance Gas model and thus do not need any root finding when solving for their ideal thermodynamic observables.

In [1], illustrations are only given for the behavior of the VDW-HRG model under the condition that the chemical potential is set to zero. Thus in Sec. 3.1, plots of different observables are shown which have the chemical potential set to zero and use the same van der Waals parameters that were found by Samanta and Mohanty. These plots only show results for a few select values of the temperature. This was done as it takes a long time for Mathematica to numerically root find for a large number of temperatures with the equations mentioned in the previous paragraph. In Sec. 3.3, we will show results for observables that were calculated not just using smaller intervals and a larger range of temperatures, but also using finite values of chemical potential. Because Mathematica is such a high level program, it is difficult to run intensive jobs quickly. Because of this, the results given in Sec. 3.3 were calculated using the C programming language. Using C instead of Mathematica, despite being much faster, turned out to be much more convoluted, specifically when trying to numerically find the roots to Eqs. (7) and (9).

In order to find the roots to Eqs. (7) and (9) using C, the Newton-Raphson method was utilized. This method is one of the simplest ways to find roots of multidimensional functions and can be very

efficient provided that you give the method a sufficiently good initial guess for the roots. A typical problem applicable for this method gives N functional relations to be zeroed, involving variables $x_i, i = 1, 2, ..., N$:

$$F_i(x_1, x_2, ..., x_N) = 0 \quad i = 1, 2, ..., N. \tag{16}$$

Now let $\mathbf{x}$ denote the vector of values x_i and $\mathbf{F}$ denote the vector of functions F_i. In the neighborhood of $\mathbf{x}$, each function F_i can be expanded into a Taylor series

$$F_i(\mathbf{x} + \delta\mathbf{x}) = F_i\mathbf{x} + \sum_{j=1}^{N} \frac{\partial F_i}{\partial x_j}\delta x_j + O(\delta\mathbf{x}^2). \tag{17}$$

The matrix of partial derivatives that appears in Eq. (17) is called the Jacobian matrix $\mathbf{J}$,

$$J_{ij} \equiv \frac{\partial F_i}{\partial x_j}. \tag{18}$$

Thus in matrix notation, Eqs. (17) and (18) become

$$\mathbf{F}(\mathbf{x} + \delta\mathbf{x}) = \mathbf{F}(\mathbf{x}) + \mathbf{J} \cdot \delta\mathbf{x} + O(\delta\mathbf{x}^2). \tag{19}$$

If we then neglect terms of second order and higher and then set $\mathbf{F}(\mathbf{x}+\delta\mathbf{x}) = 0$, we obtain a set of linear equations for the correction terms $\delta\mathbf{x}$, which simultaneously move each function F_i closer to zero. Setting $\mathbf{F}(\mathbf{x} + \delta\mathbf{x})$ results in the matrix equation

$$\mathbf{J} \cdot \delta\mathbf{x} = -\mathbf{F}(\mathbf{x}), \tag{20}$$

which can then be solved using LU decomposition. The correction terms $\delta\mathbf{x}$ are then added to the solution vector,

$$\mathbf{x}_{new} = \mathbf{x}_{old} + \delta\mathbf{x}, \tag{21}$$

and the process is reiterated until the convergence criterion is satisfied.

In our implementation of the Newton-Raphson method, both the functions F_i and the variables x_i are the VDW pressure and number density functions. This is due to the VDW pressure and number density being dependent on one another, i.e. they are transcendental equations. The code used for this method was provided by the Numerical Recipes in C library. For each value of the chemical potential and temperature, the initial starting value for each iteration of the method was set to zero as the correct initial root for the VDW pressure and number density should be the closest one to zero. In some cases, specifically at high chemical potentials, the number density and pressure of the antibaryons were so small that the method would take a very long time to converge. To circumvent this, the pressure and number density of the antibaryons were set to zero after a certain threshold ratio of the observable values of the baryons versus those of the antibaryons got too large. Another problem came at small temperatures, in the 30-55 MeV range, where at small chemical potentials the method failed to converge. This same problem also happened at very large temperatures, $T > 200MeV$. To mediate this issue, the tolerances for the different convergence criteria had to be dynamically altered depending on what temperature the iterations were working at.

In order to calculate the integrals in Eqs. (3) and (5) numerically, the technique of Gaussian quadrature was used. Gaussian quadrature is a type of quadrature rule that approximates a definite integral by using a weighted sum of function values from specified points within the integration domain. There are several different types of Gaussian quadrature rules depending on the limits of integration and the form of the function being integrated. Because of the exponential suppression in the integrals in both Eq. (3) and (5), we can get a good approximation by only integrating over a definite region of the function space. In our case, we integrated over the range [-5000, 5000] as opposed to integrating over [-∞, ∞]. After this change of limits is done, we can use the following transformation to change the limits of integration to [-1,1] which is required to perform Gaussian quadrature,

$$\int_a^b f(x)dx = \frac{b-a}{2}\int_{-1}^{1} f\Big(\frac{b-a}{2}\epsilon + \frac{a+b}{2}\Big)d\epsilon. \tag{22}$$

This can then be applied to N-point Gaussian quadrature using the following approximation,

$$\int_a^b f(x)dx \approx \frac{b-a}{2}\sum_{i=1}^{N} w_i f\Big(\frac{b-a}{2}\epsilon + \frac{a+b}{2}\Big) \tag{23}$$

The specific method of Gaussian quadrature that was used for this is called 10-point Gauss-Legendre integration and involves approximating the functions inside the integrals with Legendre polynomials. As with the Newton-Raphson method code, the code used for the Gaussian quadrature technique was provided by the Numerical Recipes in C library.

3 Results and Analysis

3.1 VDW-HRG at $\mu = 0$

In this section, results will be presented for two different sets of the VDW parameters a and b. For the first set, results using the VDW parameters found in [1] will be shown for the thermodynamic observables mentioned in Sec. 2.2 at zero chemical potential. In the second set, the same observables at zero chemical potential will be shown for the smaller VDW parameter values found in [5]. To determine the success of our implementation of the VDW-HRG model, a comparison will be made between our first set of results and the results from [1].

In Fig. 2 below, results are shown for the normalized pressure, p/T^4. Figure 2a shows our results for the VDW-HRG pressure in blue and the ideal HRG pressure in red for 30 different values of temperature in the range 100-180 MeV. At approximately 155 MeV, which is at the lower end of the QCD crossover temperature range, the ideal pressure begins to deviate from the VDW pressure. Although it is difficult to see, Samanta's results in Fig. 2b for the VDW and ideal pressure show the same deviation at around the same temperature.

The blue bands in Fig. 2b result from the errors found in [1] for the VDW parameters. These errors were found to be ± 150 MeV fm^3 and ± 0.05 fm for the attractive and radius parameters respectively. From Fig. 2b, it is apparent that until about 155 MeV, both the ideal and VDW models agree well with LQCD. However at higher temperatures, both the ideal and VDW pressure begin to deviate and underestimate LQCD data, with the VDW pressure underestimating LQCD data to a slightly greater degree than the ideal pressure. However, both curves are still consistent with LQCD results within the error-bars. For all temperatures considered, our result for the VDW pressure agrees closely with the values for the VDW pressure obtained from [1] which suggests our implementation of the VDW-HRG model was successful.

The next thermodynamic observable considered is the normalized energy density, ϵ/T^4. In Fig. 3a, the normalized energy density is shown for our implementation of the VDW-HRG model in blue and the ideal HRG model in red. In 3b, the result for normalized energy density from [1] is shown

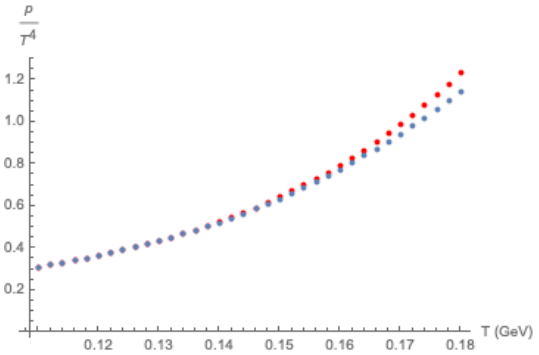

(a) Our result for the normalized pressure in the VDW-HRG model (in blue) and the ideal HRG model (in red).

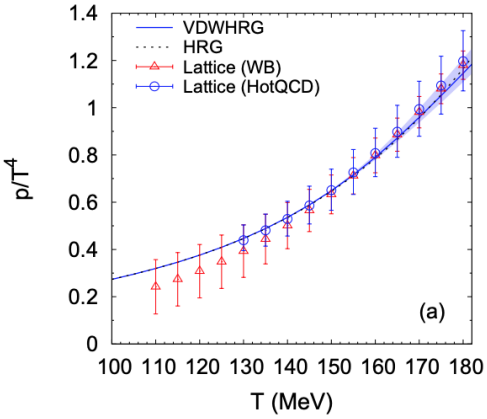

(b) Samanta and Mohanty's result for the normalized pressure in the VDW-HRG model (solid line) and the ideal HRG model (dashed line). [1]

Figure 2: In both plots, the normalized pressure, $\frac{p}{T^4}$, is shown using a=162.75 GeV^{-2} and b=748 GeV^{-3} for the VDW-HRG model and $a = b = 0$ for the ideal HRG model. In Fig. 2b, LQCD results are shown from the Wuppertal-Budapest (WB) Collaboration [2] and the HotQCD Collaboration [3].

along with LQCD results from the WB and HotQCD collaborations. In Fig. 3a, the VDW energy density begins to deviate from the ideal energy density around 155 MeV, much like the pressure. Unlike the pressure, it is much easier to see deviations between the ideal HRG model and LQCD data in Fig. 3b starting around 155 MeV which become larger at higher temperatures.

In Fig. 3b, the ideal energy density follows more closely to both sets of LQCD data than the VDW energy density does at higher temperatures. Despite this, from about 150-173 MeV the ideal energy density still underestimates the LQCD data until it reaches temperatures greater than 173 MeV where it begins to slightly overestimate LQCD data. It is expected that the ideal energy density would continue exponentially increasing at higher and higher temperatures which is not the trend of the LQCD data. The general behavior and trend of the VDW energy density closely resembling the qualitative behavior of the LQCD data indicates that at very high temperatures, the energy density is very much impacted by VDW interactions between pairs of baryons and antibaryons. A possible reason behind the suppression of the VDW energy density compared with LQCD data is the exclusion of meson interactions which were ignored in this thesis and in [1] but

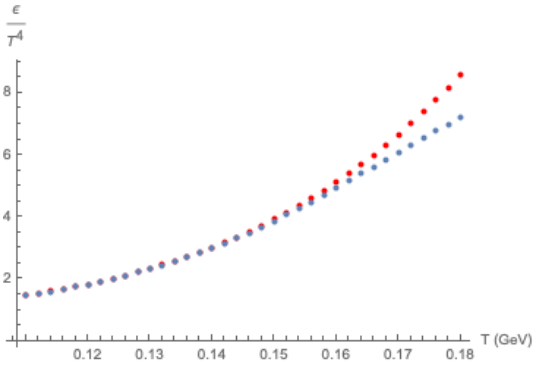

(a) Our result for the normalized energy density in the VDW-HRG model (in blue) and the ideal HRG model (in red).

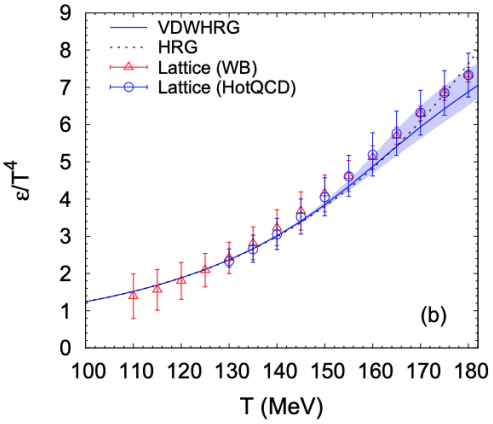

(b) Samanta and Mohanty's result for the normalized pressure in the VDW-HRG model (solid line) and the ideal HRG model (dashed line). [1]

Figure 3: Results for the normalized energy density, ϵ/T^4, at $\mu = 0$ are shown using a=162.75 GeV^{-2} and b=748 GeV^{-3} for the VDW-HRG model shown in blue in 3a and as a solid line in 3b.

could be explored in future research. Again, as was the case with the pressure, our result for the VDW energy density in Fig. 3a follows closely with the VDW energy density in Fig. 3b which further verifies the success of our implementation of the VDW-HRG model.

Figure 4 shows results for the quantity $(\epsilon - 3p)/T^4$. The reason behind the inclusion of this figure is that this quantity more clearly illustrates how at high temperatures, the trend of the ideal HRG model vastly differs from that of both the LQCD data and the VDW-HRG model. As mentioned in the previous paragraph, the qualitative behavior of the VDW-HRG model closely matches that of the LQCD data which highlights the importance of the VDW interactions at high temperatures. Whether the deviation that still exists between the VDW-HRG model and LQCD data can be remedied by inclusion of mesonic interactions remains to be seen in future research.

Figure 5 shows results for the normalized entropy density. Like the pressure and energy density, deviations begin to appear between the ideal HRG model and the VDW-HRG model at a temperature around 155 MeV. The behavior of both the ideal and VDW model versus that of the LQCD data shown in Fig. 5b mirror the behaviors observed in Figs. 3b and 4b. In Fig. 6 we have shown the results for the speed of sound squared, c_s^2. This quantity is very important in the

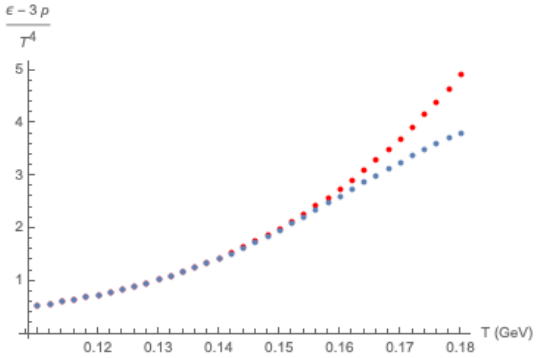

(a) Result for the VDW-HRG model is shown in blue and the ideal HRG model in red.

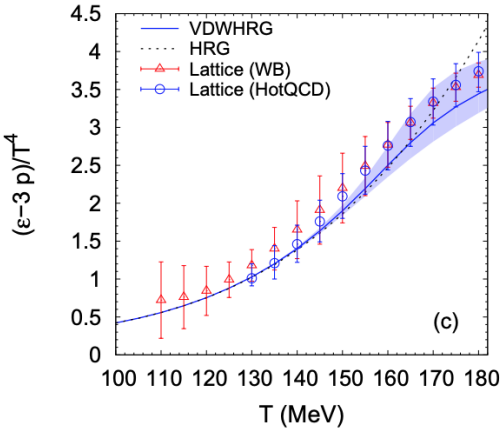

(b) Result for the VDW-HRG model is shown with the solid line and with a dashed line for the ideal HRG model. [1]

Figure 4: The quantity shown in these two figures helps highlight the deviation of the ideal HRG model from LQCD data and the VDW-HRG model at high temperatures which became apparent in Fig. 3.

study of phase transitions and happens to be the most interesting observable calculated using the VDW-HRG model.

Looking at Fig. 6b, one can see that, as the system moves to higher temperatures, the ideal c_s^2 decreases linearly which is nothing like what happens with LQCD data. However, using the VDW-HRG model result for c_s^2 almost exactly replicates LQCD data. Both LQCD and VDW-HRG show a minimum around T=150-155 MeV. This minimum is known as the softest point in the expansion and is a result of the expansion of the system slowing down. Because of this, the system spends a longer time in this temperature range and could indicate the phase transition of hadronic matter into the QGP [4].

The final observable that we have included in our analysis of the VDW-HRG model at μ=0 is shown below in Fig. 7. This quantity is the specific heat at constant volume and measures the rate of change in energy density w.r.t. temperature, at constant volume. For this observable, the VDW-HRG model is in very close agreement with LQCD data at high temperatures whereas the ideal HRG model overestimates and exponentially increases. This same type of behavior has been seen in nearly every other observable considered in this analysis. Again, as with the other

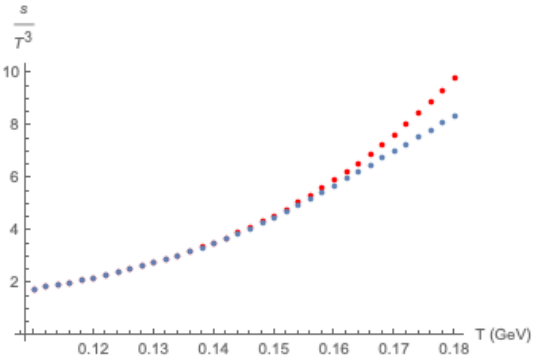

(a) Normalized entropy density results for VDW-HRG model shown in blue and the ideal HRG model shown in red.

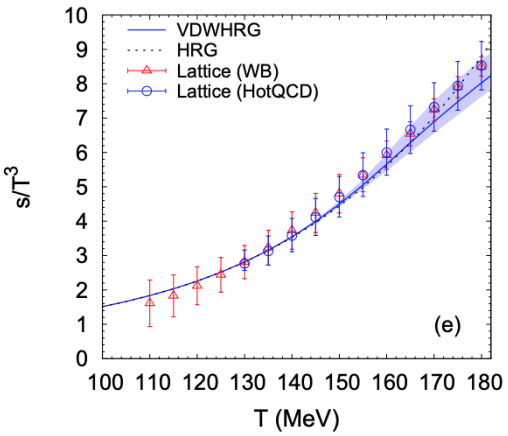

(b) Samanta and Mohanty's result for the normalized entropy density in the VDW-HRG model (solid line) and the ideal HRG model (dashed line).

Figure 5: Results for the normalized entropy density at $\mu = 0$ are shown using a=162.75 GeV^{-2} and b=748 GeV^{-3} for the VDW-HRG model shown in blue in 5a and as a solid line in 5b.

observables analyzed, our implementation of the VDW-HRG model closely aligns with the results obtained for the model in [1] which suggests that our implementation was successful.

In Figs. 8 and 9, we have included results for each of the observables shown in Figs. 2-7 but now instead of using the VDW parameter values found in [1], we use the values found in [5]. These new values were found by fitting the VDW-HRG model with the ground state properties of nuclear matter and came out to be a=329 MeV fm^3 and b=3.42 fm^3 (r=0.59 fm) which are both considerably smaller than those found in [1]. Looking at Fig. 8a, it appears that the smaller VDW parameters lead to the VDW-HRG model staying nearer in value to the ideal HRG model even at high temperatures. Of course this is what is expected not just for the pressure but for all observables as the ideal HRG model is just the limit of the VDW-HRG model as the VDW parameters approach zero. In addition, Figs. 8a-8c and 9b all show a deviation between the two models around a temperature of 155 MeV, which is what was also illustrated in Figs. 2-7. Two differences that stick out are that the speed of sound squared, c_s^2, in Fig. 9a has a minimum around 160 MeV as opposed to 150-155 MeV in Fig. 6a and that there isn't a noticeable hump in the normalized specific heat at constant volume, C_V/T^3, in Fig. 9c around T=160 MeV, which was

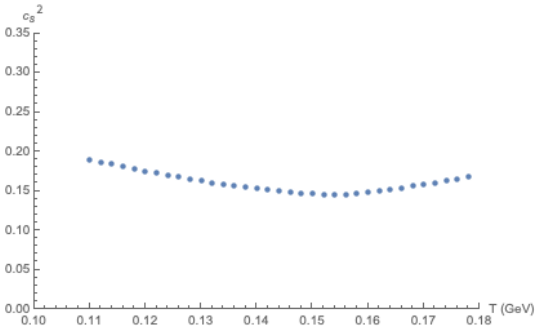

(a) Result for the speed of sound squared, c_s^2, using our implementation of the VDW-HRG model.

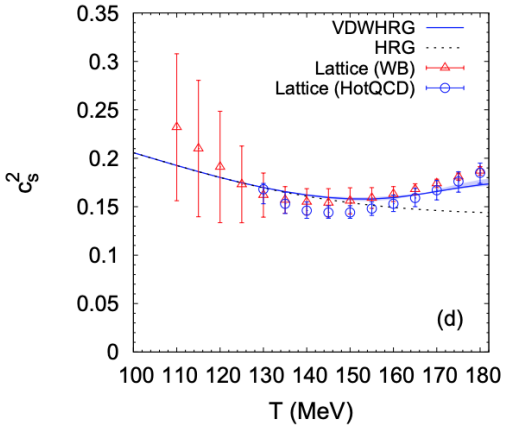

(b) Samanta and Mohanty's results for c_s^2 using the VDWHRG model (solid line) and the ideal HRG model (dashed line).

Figure 6: Results for the speed of sound squared, c_s^2, at $\mu = 0$ are shown using a=162.75 GeV^{-2} and b=748 GeV^{-3} for the VDW-HRG model shown in blue in 5a and as a solid line in 5b. This quantity is very important to the study of the QCD phase diagram as it is sensitive to phase transitions [4].

the case in Fig. 7a.

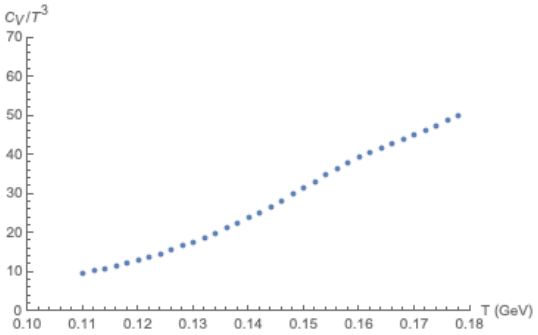

(a) Our result for the normalized specific heat at constant volume, C_V/T^3.

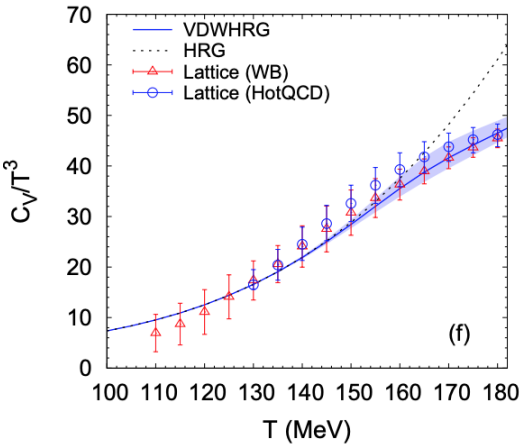

(b) Samanta and Mohanty's results for C_V/T^3.

Figure 7: Results for C_V/T^3, at $\mu = 0$ are shown using a=162.75 GeV^{-2} and b=748 GeV^{-3} for the VDW-HRG model shown in blue in 6a and as a solid line in 6b. The ideal HRG result for C_V/T^3 is shown as a dashed line in 6b.

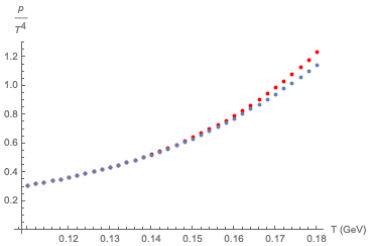

(a) Result for the normalized pressure in the VDW-HRG model (in blue) and the ideal HRG model (in red).

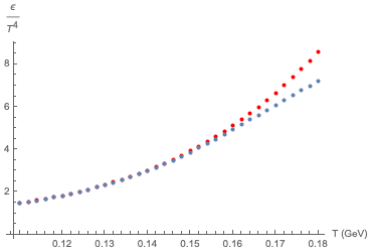

(b) Result for the normalized energy density in the VDW-HRG model (in blue) and the ideal HRG model (in red).

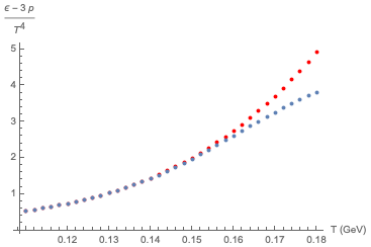

(c) Result for $(\epsilon - 3p)/T^4$ with the VDW-HRG model is shown in blue and the ideal HRG model in red.

Figure 8: Results are shown for the normalized pressure, energy density and the quantity $(\epsilon - 3p)/T^4$ using both the ideal HRG and VDW-HRG models. The results for the VDW-HRG model are calculated using a=42.8 GeV^{-2} and b=445.2 GeV^{-3} which are the VDW parameter values found in [5].

3.2 VDW-HRG at finite μ

In this section, results will be presented for the VDW-HRG model while including finite values of the chemical potential in the calculations. These results were all calculated using code written in C and then plotted using Mathematica. This was done so that a much broader range of temperatures

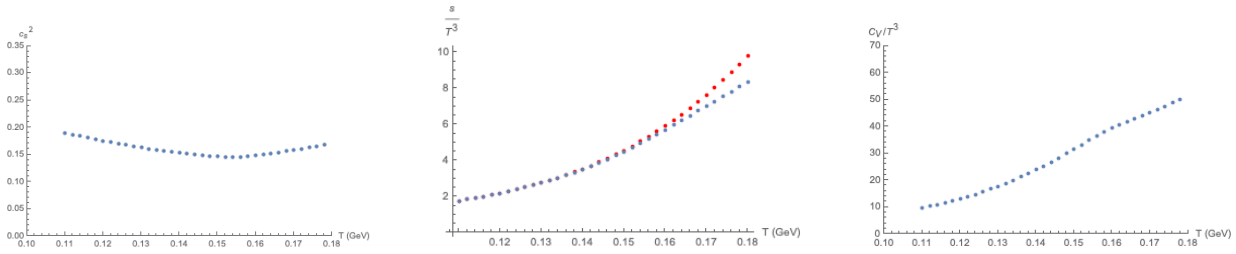

(a) Result for the speed of sound squared, c_s^2, using the VDW-HRG model.

(b) Results for the normalized entropy density using the VDW-HRG model (in blue) and the ideal HRG model (in red).

(c) Result for the normalized specific heat at constant volume, C_V/T^3, using the VDW-HRG model.

Figure 9: Results are shown for the speed of sound squared, normalized entropy density and the normalized specific heat at constant volume. The results for the VDW-HRG model are calculated using a=42.8 GeV^{-2} and b=445.2 GeV^{-3} which are the VDW parameter values found in [5].

could be probed, in addition to examining a very large range of chemical potential values.

In Fig. 10, two different images of the plot for the normalized total pressure are shown. The left plot, Fig. 10a, shows the total normalized pressure over a temperature range of 30 to 250 MeV amd a chemical potential range of 0 to 1300 MeV. In this image, we see that the total pressure exponentially increases as a function of both temperature and chemical potential, which is expected.

The plot in Fig. 10b is a result of cutting the pressure off at a certain value and then looking at

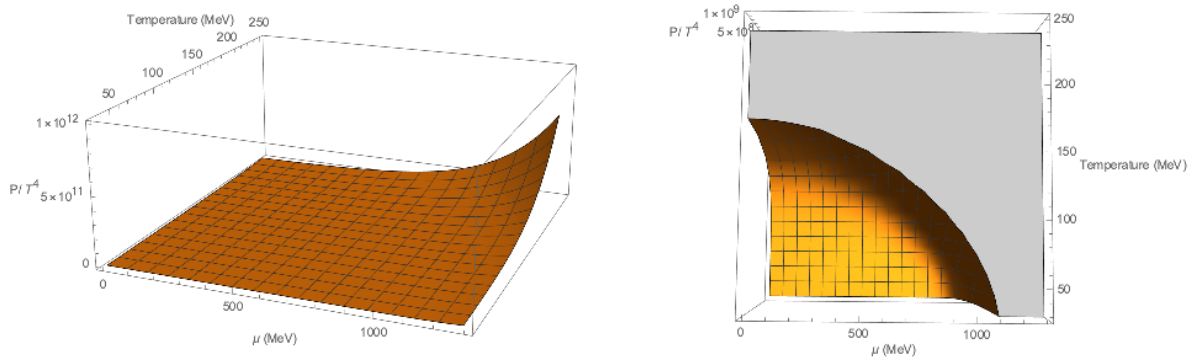

(a) Result for the normalized total pressure using the VDW-HRG model.

(b) Top down view of Fig. 10a.

Figure 10: Result for the normalized total pressure using the VDW parameters from [1] for a temperature range of 30-250 MeV and chemical potential range of 0-1300 MeV.

a top down view of the T-μ_B plane. The cutoff value was chosen such that the top down view on

the T-μ_B plane could give an example illustration of what the pressure may look like on the QCD phase diagram (see Fig. 1), where at the phase transition, the pressure would exponentially jump due to quark deconfinement.

In Fig. 11, similar results are shown for the normalized net baryon density, which takes on positive values when there are more baryons than antibaryons in the system and vice versa for negative values. Figure 11a shows a result very similar to the pressure in Fig. 10a, where there is an exponential increase as the system moves towards higher temperatures and chemical potentials. One interesting characteristic of Fig. 11b is that, as the system moves towards zero chemical potential and very high temperatures, the 3D-curve for the net baryon density gets infinitesimally close to touching the $(n/T^3) - T$ plane. This occurs because as the system approaches higher temperatures, more net baryons are produced at smaller and smaller chemical potentials. However, as the system approaches zero chemical potential, the system must produce no net baryon (or antibaryons), regardless of how high the temperature becomes.

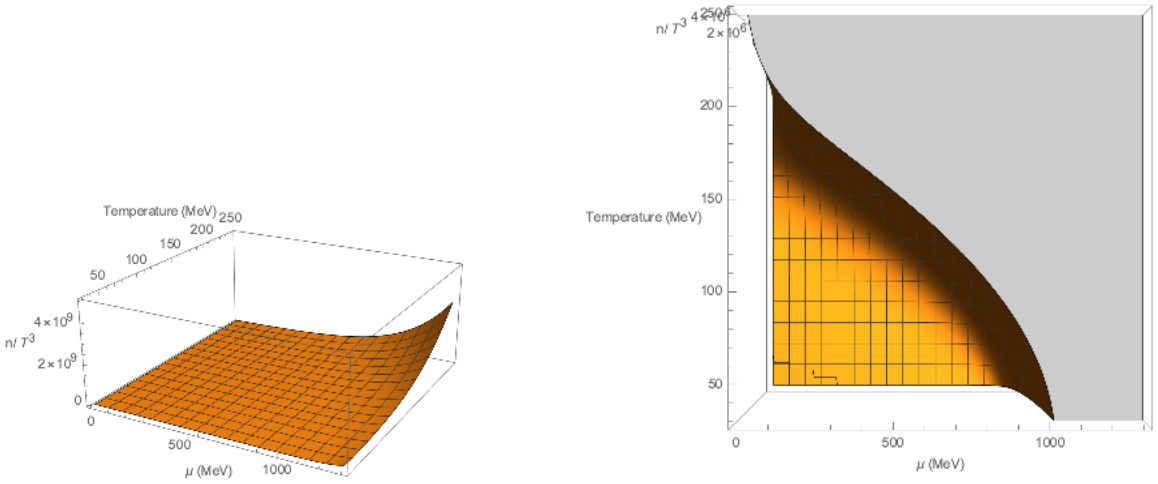

(a) Result for the normalized net baryon density using the VDW-HRG model.

(b) Top down view of Fig. 11a.

Figure 11: Result for the normalized net baryon density using the VDW parameters from [1] for a temperature range of 30-250 MeV and chemical potential range of 0-1300 MeV.

In Figs. 12 and 13, results are shown for the normalized energy and entropy densities respectively. For these sets of plots, the respective observables were only calculated for a temperature

range of 30 to 210 MeV and a chemical potential range of 0 to 1300 MeV. We were unable to reach the extreme temperatures above 210 MeV that were shown in Figs. 10 and 11 due to convergence issues. Both results show very little dependence on the chemical potential and have a slowly increasing trend as the system moves towards high temperatures. In Figs. 12b and 13b, there is a small noticeable dependence on the chemical potential at temperatures above 170 MeV. More specifically, both the energy and entropy density begin to increase faster at larger chemical potentials when the temperatures are greater than ∼170 MeV.

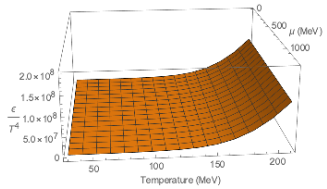

(a) Result for the normalized energy density density using the VDW-HRG model.

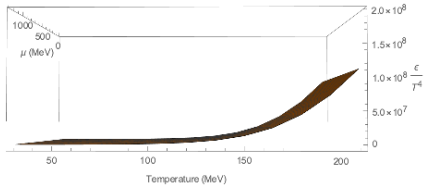

(b) Side view of Fig. 12a along the temperature axis.

Figure 12: Result for the normalized energy density using the VDW parameters from [1] for a temperature range of 30-210 MeV and chemical potential range of 0-1300 MeV.

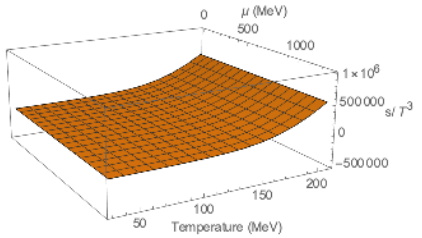

(a) Result for the normalized entropy density using the VDW-HRG model.

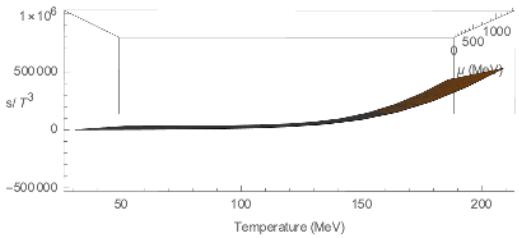

(b) Side view of Fig. 13a along the temperature axis.

Figure 13: Result for the normalized entropy density using the VDW parameters from [1] for a temperature range of 30-210 MeV and chemical potential range of 0-1300 MeV.

The final observable result for the VDW-HRG model at finite chemical potential is shown in Fig. 14. The observable shown is the second order fluctuation of baryon number, χ_B^2, and is the second derivative of the total normalized pressure with respect to the normalized baryon chemical potential, see Eq. (15). Because both pressure and chemical potential are normalized by the

temperature, Fig. 14 shows a dependence on the temperature even though it is derivative with respect to the chemical potential.

Disregarding the $\frac{1}{T^3}$ suppression for χ_B^2 from Eq. (15), we can compare Fig. 14 to the behavior of the pressure in Fig. 10a. From Fig. 10a, the second derivative of the pressure with respect to μ_B should be small for all temperatures at low μ_B which Fig. 14 clearly shows. In addition, the second derivative should be positive for all temperatures at high μ_B, with the most positive being at very high temperatures. However, Fig. 14 shows that the most positive value of χ_B^2 is at low temperatures and high μ_B. This disagreement is due to the $\frac{1}{T^3}$ suppression in Eq. (15) which results from using the normalized pressure and chemical potential. Thus, by comparison with Fig. 10a, our result for χ_B^2 in Fig. 14 is consistent with the pressure results. The reason for including χ_B^2 in these results is because in [1], one of the observables used to extract the van der Waals parameters was χ_B^2 at zero chemical potential. A plot of χ_B^2 at $\mu_B = 0$ using the VDW-HRG model, which shows remarkable agreement with LQCD data, can be seen in Fig. 2 of [1].

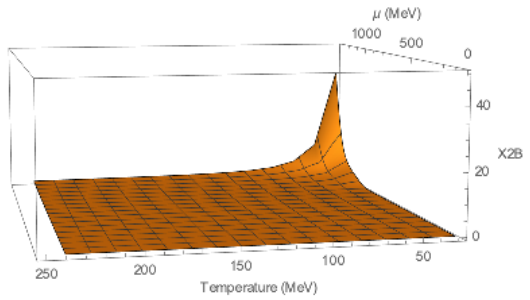

Figure 14: Result for the second order fluctuation of baryon number, χ_B^2, using the VDW parameters from [1] for a temperature range of 30-250 MeV and chemical potential range of 0-1300 MeV.

4 Conclusions

The primary goal of this thesis was to implement van der Waals interactions into the ideal Hadron Resonance Gas (HRG) model, creating the VDW-HRG model. This was done to improve the ability for the HRG model to reproduce Lattice QCD results over a larger range of temperatures. In Chapter 1, a general introduction to the field was given, along with brief descriptions of the various methods in which the Quark-Gluon plasma has been studied. In Chapter 2, a description of the HRG model and how to include van der Waals interactions into the model was presented. In addition, a technical description of how the VDW-HRG model was implemented in this thesis was given.

In Chapter 3, results were presented for several thermodynamic observables using both the ideal HRG and the VDW-HRG model at both zero and finite chemical potential. In Sec. 3.1, the goal was to calculate observables such as pressure and energy density at zero chemical potential using our implementation of the VDW-HRG model and then compare our results to those of [1]. In order to make the comparison, we used the same van der Waals parameters that were found in Samanta and Mohanty's paper by fitting the VDW-HRG model with Lattice QCD data.

Through this comparison, it became apparent that our implementation of the VDW-HRG model was successful as the values and behaviors of our calculations for select thermodynamic observables matched those from [1]. In addition, in Sec. 3.1, results were presented for the VDW-HRG model using the van der Waals parameters found by fitting the VDW-HRG model with the ground state properties of nuclear matter in [5] which allowed for a comparison between the behavior of observables for the two sets of van der Waals parameters. In Sec. 3.2, results for the VDW-HRG model at finite chemical potential were given. These results are consistent with what is expected for the behaviors of the various thermodynamic observables shown at finite chemical potential and once again indicate that our implementation of the VDW-HRG model was successful. In future research, the results presented in this thesis for the VDW-HRG model will be used to give a more realistic description of the matter created in heavy ion collisions at finite temperature and chemical

potential. Possible extensions to the version of the VDW-HRG model used in this thesis, which could include accounting for mesonic interactions or incorporating temperature dependent van der Waals parameters, may also be explored in future research, in the hope of producing a closer representation to LQCD data.

Bibliography

[1] Subhasis Samanta and Bedangadas Mohanty. Criticality in a Hadron Resonance Gas model with the van der Waals interaction, 2017.

[2] Szabolcs Borsányi, Zoltán Fodor, Christian Hoelbling, Sándor D. Katz, Stefan Krieg, and Kálmán K. Szabó. Full result for the QCD equation of state with 2+1 flavors. *Physics Letters B*, 730:99–104, 2014.

[3] A. Bazavov *et al*. [Hot QCD Collaboration]. Equation of state in $(2+1)$-flavor qcd. *Phys. Rev. D*, 90:094503, Nov 2014.

[4] C. M. Hung and E. V. Shuryak. Hydrodynamics near the qcd phase transition: Looking for the longest-lived fireball. *Physical Review Letters*, 75(22):4003–4006, Nov 1995.

[5] V. Vovchenko, D. V. Anchishkin, and M. I. Gorenstein. Van der Waals equation of state with Fermi statistics for nuclear matter. *Phys. Rev. C*, 91:064314, Jun 2015.

[6] D.J. Schwarz. The first second of the Universe. *Annalen der Physik*, 12(4):220–270, 2003.

[7] M. Gell-Mann. The Eightfold Way: A theory of Strong Interaction Symmetry. Pasadena, CA: California Inst. of Tech., Synchrotron Laboratory, Mar 1961.

[8] M. Gell-Mann. A schematic model of baryons and mesons. *Physics Letters*, 8(3):214–215, February 1964.

[9] G Zweig. An SU(3) Model for Strong Interaction Symmetry and its Breaking. *CERN Report No.8182/TH.401 and No.8419/TH.412*, 1964.

[10] O. W. Greenberg. Spin and Unitary-Spin Independence in a Paraquark Model of Baryons and Mesons. *Phys. Rev. Lett.*, 13(20):598–602, Nov 1964.

[11] David J. Gross and Frank Wilczek. Ultraviolet Behavior of Non-Abelian Gauge Theories. *Phys. Rev. Lett.*, 30(26):1343–1346, Jun 1973.

[12] H. David Politzer. Reliable Perturbative Results for Strong Interactions? *Phys. Rev. Lett.*, 30(26):1346–1349, Jun 1973.

[13] Frank Wilczek. Asymptotic Freedom: From Paradox to Paradigm. Dec 2004.

[14] Thomas Schäfer and Derek Teaney. Nearly perfect fluidity: from cold atomic gases to hot quark gluon plasmas. *Reports on Progress in Physics*, 72(12):126001, Nov 2009.

[15] Edward Shuryak. Physics of strongly coupled quark–gluon plasma. *Progress in Particle and Nuclear Physics*, 62(1):48–101, Jan 2009.

[16] M BUBALLA. Njl-model analysis of dense quark matter. *Physics Reports*, 407(4-6):205–376, Feb 2005.

[17] D Rischke. The quark–gluon plasma in equilibrium. *Progress in Particle and Nuclear Physics*, 52(1):197–296, Mar 2004.

[18] A. Bazavov, H.-T. Ding, P. Hegde, O. Kaczmarek, F. Karsch, E. Laermann, Y. Maezawa, Swagato Mukherjee, H. Ohno, P. Petreczky, and et al. Qcd equation of state to o(b6) from lattice qcd. *Physical Review D*, 95(5), Mar 2017.

[19] Bastian Brandt and G. Endrődi. Reliability of taylor expansions in qcd. *Physical Review D*, 99, 01 2019.

[20] M. A. Stephanov. QCD phase diagram: an overview, 2006.

[21] N. Cabibbo and G. Parisi. Exponential Hadronic Spectrum and Quark Liberation. *Phys. Lett.*, 59B:67–69, 1975.

[22] J. C. Collins and M. J. Perry. Superdense matter: Neutrons or asymptotically free quarks? *Phys. Rev. Lett.*, 34:1353–1356, May 1975.

[23] J. Schukraft. Ultrarelativistic heavy ion collisions: Searching for the quark - gluon plasma. *Nucl. Phys. News*, 2:14–21, 1992.

[24] Jurgen Schukraft and Reinhard Stock. Toward the Limits of Matter: Ultra-relativistic nuclear collisions at CERN. *Adv. Ser. Direct. High Energy Phys.*, 23:61–87, 2015.

[25] Reinhard Stock. 7 relativistic nucleus-nucleus collisions and the qcd matter phase diagram. *Landolt-Börnstein - Group I Elementary Particles, Nuclei and Atoms*, page 225–315, 2008.

[26] Ulrich Heinz and Maurice Jacob. Evidence for a new state of matter: An assessment of the results from the cern lead beam programme, 2000.

[27] J. Adams, M.M. Aggarwal, Z. Ahammed, J. Amonett, B.D. Anderson, D. Arkhipkin, G.S. Averichev, S.K. Badyal, Y. Bai, J. Balewski, and et al. Experimental and theoretical challenges in the search for the quark–gluon plasma: The star collaboration's critical assessment of the evidence from rhic collisions. *Nuclear Physics A*, 757(1-2):102–183, Aug 2005.

[28] K. Adcox et al. Formation of dense partonic matter in relativistic nucleus-nucleus collisions at RHIC: Experimental evaluation by the PHENIX collaboration. *Nucl. Phys.*, A757:184–283, 2005.

[29] B.B. Back, M.D. Baker, M. Ballintijn, D.S. Barton, B. Becker, R.R. Betts, A.A. Bickley, R. Bindel, A. Budzanowski, W. Busza, and et al. The phobos perspective on discoveries at rhic. *Nuclear Physics A*, 757(1-2):28–101, Aug 2005.

[30] I. Arsene et al. Quark gluon plasma and color glass condensate at RHIC? The Perspective from the BRAHMS experiment. *Nucl. Phys.*, A757:1–27, 2005.

[31] R. Nouicer. New State of Nuclear Matter: Nearly Perfect Fluid of Quarks and Gluons in Heavy Ion Collisions at RHIC Energies. *Eur. Phys. J. Plus*, 131(3):70, 2016.

[32] Declan Keane. The Beam Energy Scan at the Relativistic Heavy Ion Collider. *Journal of Physics: Conference Series*, 878(1-2):102–183, Jul 2017.

[33] Grazyna Odyniec. Beam Energy Scan Program at RHIC (BES I and BES II) – Probing QCD Phase Diagram with Heavy-Ion Collisions. *PoS*, CORFU2018:151, 2019.

[34] Y. Nambu and G. Jona-Lasinio. Dynamical model of elementary particles based on an analogy with superconductivity. i. *Phys. Rev.*, 122:345–358, Apr 1961.

[35] Y. Nambu and G. Jona-Lasinio. Dynamical model of elementary particles based on an analogy with superconductivity. ii. *Phys. Rev.*, 124:246–254, Oct 1961.

[36] A. Chodos, R. L. Jaffe, K. Johnson, C. B. Thorn, and V. F. Weisskopf. New extended model of hadrons. *Phys. Rev. D*, 9:3471–3495, Jun 1974.

[37] V Vovchenko, D V Anchishkin, and M I Gorenstein. Particle number fluctuations for the van der Waals equation of state. *Journal of Physics A: Mathematical and Theoretical*, 48(30):305001, Jul 2015.

[38] Subhasis Samanta and Bedangadas Mohanty. Estimation of attractive and repulsive interactions from the fluctuation observables at RHIC using van der Waals hadron resonance gas Model, 2019.

[39] Rameez Ahmad Parra, Saeed Uddin, Waseem Bashir, and Inam ul Bashir. Thermal Model Calculations for Hot and Dense Hadronic Matter Using van der Waals Type Equation of State, 2019.

[40] R. Poberezhnyuk, V. Vovchenko, A. Motornenko, M. I. Gorenstein, and H. Stoecker. Chemical freeze-out conditions and fluctuations of conserved charges in heavy-ion collisions within quantum van der waals model, 2019.

[41] Volodymyr Vovchenko, Anton Motornenko, Paolo Alba, Mark I. Gorenstein, Leonid M. Satarov, and Horst Stoecker. Multicomponent van der Waals equation of state: Applications in nuclear and hadronic physics, 2017.

[42] Szabolcs Borsányi, Zoltán Fodor, Christian Hoelbling, Sándor D Katz, Stefan Krieg, and Kálmán K Szabó. Full result for the QCD equation of state with 2+1 flavors. *Physics Letters B*, 730(C):99–104, 2014.

[43] R. Bellwied, S. Borsanyi, Z. Fodor, S. D. Katz, A. Pasztor, C. Ratti, and K. K. Szabo. Fluctuations and correlations in high temperature QCD, 2015.

[44] H A Bethe. Theory of Nuclear Matter. *Annual Review of Nuclear Science*, 21(1):93–244, 1971.

[45] He-Xia Zhang, Jin-Wen Kang, and Ben-Wei Zhang. In-medium effect on the thermodynamics and transport coefficients in van der Waals hadron resonance gas, 2019.

[46] C. Patrignani et al. Review of Particle Physics. *Chin. Phys.*, C40(10):100001, 2016.